

# Worst Case Power/Ground Noise Estimation Using an Equivalent Transition Time for Resonance

Emre Salman, *Student Member, IEEE*, Eby G. Friedman, *Fellow, IEEE*, Radu M. Secareanu, *Member, IEEE*, and Olin L. Hartin

**Abstract**—The nonmonotonic behavior of power/ground noise with respect to the transition time  $t_r$  is investigated for an inductive power distribution network with a decoupling capacitor. The worst case power/ground noise obtained with fast switching characteristics is shown to be significantly inaccurate. An equivalent transition time that corresponds to resonance is presented to accurately estimate the worst case power/ground noise in the time domain. Furthermore, the sensitivity of the ground noise to the decoupling capacitance  $C_d$  and parasitic inductance  $L_g$  is evaluated as a function of the transition time. Increasing the decoupling capacitance is shown to efficiently reduce the noise for transition times smaller than twice the  $LC$  time constant,  $t_r \leq 2\sqrt{L_g C_d}$ . Alternatively, reducing the parasitic inductance  $L_g$  is shown to be effective for transition times greater than twice the  $LC$  time constant,  $t_r \geq 2\sqrt{L_g C_d}$ . The peak noise occurs when the transition time is approximately equal to twice the  $LC$  time constant,  $t_r \approx 2\sqrt{L_g C_d}$ , referred to as the equivalent transition time for resonance.

**Index Terms**—Decoupling capacitance, noise reduction, noise sensitivity, power/ground distribution network, power/ground noise, resonance, target impedance, worst case transition time.

## I. INTRODUCTION

**I**N A high-performance integrated circuit, power and ground voltages should be reliably distributed to satisfy functionality and performance while considering the overall resources devoted to these distribution networks. The reliable distribution of power and ground voltages, however, is a challenging task due to the high current demands and reduced operating voltages [1], [2]. The parasitic resistance and inductance of the power and ground distribution networks produce  $IR + L\partial i/\partial t$  voltage drops, reducing the overall voltage across the load. Efficient and sufficiently accurate estimation of these voltage drops is also challenging due to the high complexity of on-chip interconnects [3].

Typically, two design metrics should be satisfied when characterizing the power noise in the time domain [4]: 1) the max-

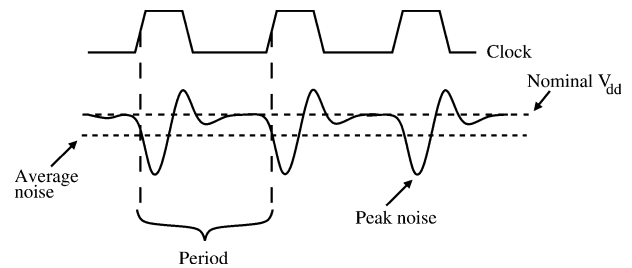


Fig. 1. Clock waveform and corresponding peak and average power noise in the time domain.

imum allowable average noise within a clock cycle and 2) the maximum allowable peak noise. The average noise determines the amount of variation in the delay of a critical path, that is, the maximum operating frequency of the circuit under power supply variations is dependent upon the average noise. The maximum allowable peak noise is determined by the noise margins. A power noise greater than the maximum noise can change the logic state of a node, causing a circuit to fail. The time domain representation of the peak and average power noise, and a related clock waveform are illustrated in Fig. 1 for a synchronous digital circuit. A significant number of registers switches simultaneously with the rising edge of the clock, causing a considerable drop in the power supply voltage during this transition time [5]. Furthermore, the noise signal can propagate to the output of a gate, degrading signal integrity and causing unnecessary power consumption [6], [7]. Power/ground noise can also affect sensitive circuits such as phase-locked loops and sigma-delta modulators by producing additional jitter [8].

Decoupling capacitors are often used to reduce power/ground noise by temporarily providing charge to the load circuits during switching events [9], [10]. Several factors such as the placement, size, and recharge time of the decoupling capacitors should be considered for efficiency [11]–[13]. Another important consideration for decoupling capacitors is the  $LC$  resonance. The parallel combination of the decoupling capacitor  $C_d$  with the parasitic inductance  $L_g$  of the power distribution network produces a peak impedance at the resonant frequency  $f = 1/(2\pi\sqrt{L_g C_d})$  due to the  $LC$  tank circuit. The impedance at the resonant frequency should therefore be smaller than the target impedance to satisfy the noise constraints.

The impedance characteristics of a power distribution system have been investigated with particular focus on the resonant behavior [14], [15]. The corresponding transition time that produces the maximum noise in the time domain, however, has not received much attention. Faster signal transitions (smaller transition times) are typically assumed to produce the worst

Manuscript received September 19, 2008; revised January 02, 2009. First published March 04, 2009; current version published May 20, 2009. This work was supported in part by the Semiconductor Research Corporation under Contract 2004-TJ-1207, the National Science Foundation under Contract CCF-0541206, grants from the New York State Office of Science, Technology and Academic Research to the Center for Advanced Technology in Electronic Imaging Systems, and by grants from Intel Corporation, Eastman Kodak Company, and Freescale Semiconductor Corporation. This paper was recommended by Guest Editor Y. Ismail.

E. Salman and E. G. Friedman are with the Department of Electrical and Computer Engineering, University of Rochester, Rochester, NY 14627 USA (e-mail: salman@ece.rochester.edu; friedman@ece.rochester.edu).

R. M. Secareanu and O. L. Hartin are with Freescale Semiconductor, Tempe, AZ 85284 USA (e-mail: r54143@freescale.com; lee.hartin@freescale.com).

Digital Object Identifier 10.1109/TCSI.2009.2016614

case noise. This assumption, however, is not valid for an inductive power distribution network with a decoupling capacitor. In [16], two extreme cases are considered in the analysis of ground noise: when the switching time is much smaller or much greater than the inverse resonant frequency. The maximum noise, however, occurs at an intermediate transition time rather than at one of the two extreme cases, as shown in this paper.

The nonmonotonic behavior of power/ground noise with respect to the transition time is investigated. The worst case transition time producing the maximum noise in the presence of a decoupling capacitor is determined. The sensitivity of the noise to the decoupling capacitance and parasitic inductance is also evaluated.

The remainder of this paper is organized as follows. Background material is provided in Section II. The equivalent circuit model to estimate the peak-to-peak power/ground noise is described in Section III. The nonmonotonic noise behavior with respect to the transition time is investigated in Section IV. The paper is concluded in Section V.

## II. BACKGROUND

Background material is provided in this section for determining the worst case transition time. Specifically, the target impedance characterizing a power distribution network is described in Section II-A. The use of a decoupling capacitor to satisfy a target impedance is explained in Section II-B. The difficulty of a frequency domain analysis and the need for a *worst case transition time* in time domain analyses are discussed in Section II-C.

### A. Target Impedance

A power distribution system is typically analyzed in the frequency domain to satisfy a *target impedance* over a specific range of operating frequency [1]. The target impedance of a power distribution network is determined from the nominal power supply voltage  $V_{\text{nom}}$ , maximum tolerable ripple  $r$  on the load circuit as a per cent of the nominal power supply voltage, and the current  $I_{\text{avg}}$  required by a load circuit from the power distribution network [10]

$$Z_{\text{target}} = \frac{V_{\text{nom}} \times r(\%)}{I_{\text{avg}}}. \quad (1)$$

The average current is estimated from the power consumption  $P$  at a specific clock frequency

$$I_{\text{avg}} = \frac{P}{V_{\text{nom}}}. \quad (2)$$

Replacing (2) in (1) results in

$$Z_{\text{target}} = \frac{V_{\text{nom}}^2 \times r(\%)}{P}. \quad (3)$$

As determined by (3), the target impedance is reduced quadratically as the nominal voltage is scaled. Furthermore, the power consumption increases due to the higher integration densities, requiring further reductions in the target impedance. A recent

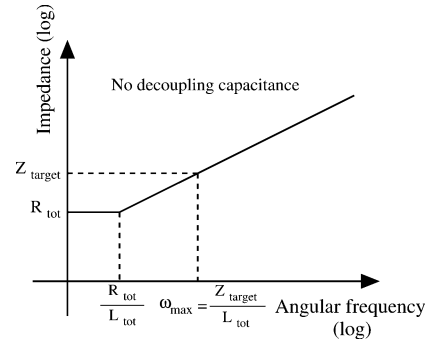


Fig. 2. Impedance characteristics of a power distribution network without a decoupling capacitor.

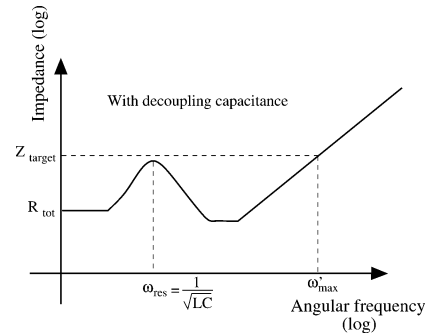


Fig. 3. Impedance characteristics of a power distribution network with a decoupling capacitor.

16 core microprocessor, implemented in a 65-nm CMOS technology, consumes 250 W at a supply voltage of 1.2 V [17]. According to (3), the impedance of the power distribution network for this microprocessor should be less than 0.3 m $\Omega$  over a wide frequency range, assuming a 5% maximum ripple is allowed, i.e.,  $r = 0.05$ . The target impedance should therefore be aggressively decreased to satisfy power/ground noise constraints in deep-submicrometer technologies.

### B. Decoupling Capacitance

Decoupling capacitances have traditionally been placed across power and ground conductors to satisfy a required target impedance [1], [18], [19]. A typical frequency response of a power distribution system with and without a decoupling capacitor is depicted, respectively, in Figs. 2 and Fig. 3 [1].

When no decoupling capacitance exists, the total resistive impedance  $R_{\text{tot}}$  dominates at frequencies  $\omega < R_{\text{tot}}/L_{\text{tot}}$ . At frequencies  $\omega > R_{\text{tot}}/L_{\text{tot}}$ , the impedance linearly increases since the total inductive impedance  $|j\omega L_{\text{tot}}|$  dominates. At the frequency  $\omega_{\text{max}} = Z_{\text{target}}/L_{\text{tot}}$ , the impedance exceeds the target impedance, as depicted in Fig. 2. A decoupling capacitor increases the frequency at which the output impedance exceeds the target impedance, as illustrated in Fig. 3 [1].

Note, however, that with a decoupling capacitor, the frequency response exhibits a nonmonotonic behavior due to resonance. Specifically, at the resonant frequency  $\omega = 1/\sqrt{LC}$ , the total impedance with a decoupling capacitance is larger than the impedance without a decoupling capacitance due to

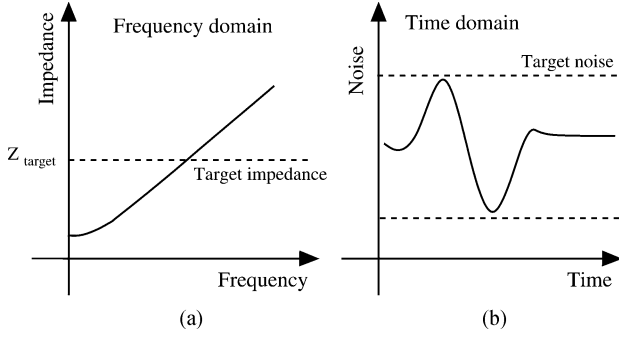


Fig. 4. Target impedance and noise. (a) Target impedance is not satisfied in the frequency domain, (b) although the target noise is satisfied in the time domain.

the parallel combination of the capacitance and inductance, forming an  $LC$  tank circuit.

In the frequency domain, the resonant frequency produces the worst case peak power noise. This nonmonotonic behavior is described here in the time domain. The advantages of a time-domain analysis are reviewed in the following subsection.

### C. Frequency-Domain Versus Time-Domain Analysis

Although computationally more efficient, a frequency-domain analysis is typically pessimistic as compared with a time-domain analysis [20] since the frequency range over which the target impedance should be satisfied is not well defined. As illustrated in Fig. 4 [20], the peak-to-peak noise can be within the tolerable range although the target impedance is not satisfied. A frequency-domain analysis therefore may cause overdesign of the power/ground network [20]. Alternatively, a time-domain analysis produces an estimate of the power/ground noise that is less pessimistic.

A primary issue in time-domain analysis is the difficulty in considering the resonant behavior. The fastest transition, i.e., smallest transition time of the current transients, is typically assumed to produce the greatest noise [16]. This assumption is not valid, as described in this paper, due to the nonmonotonic behavior of the power/ground noise. An approximate solution for the worst case transition time producing the greatest power/ground noise in the time domain is presented. The sensitivity of noise to the parasitic inductance and decoupling capacitance is also investigated as a function of transition time.

## III. POWER/GROUND NOISE MODEL

An equivalent circuit model to investigate the noise behavior in terms of the transition time is shown in Fig. 5, where  $R_p$ ,  $L_p$  and  $R_g$ ,  $L_g$  represent the power and ground impedances, respectively,  $C_d$  is the decoupling capacitor, and  $R_d$  is the effective series resistance of the capacitor. Note that  $C_d$  is the summation of the intentional decoupling capacitance and the intrinsic capacitance of the nonswitching gates within a circuit [21]. Techniques to estimate this capacitance are described in [22]. The load circuit is represented by a current source with a transition time  $t_{r,i}$  and peak current  $I_{swi,p}$ . This triangular approximation of the current waveform is reasonable since a large number of registers switches simultaneously with the clock signal in synchronous

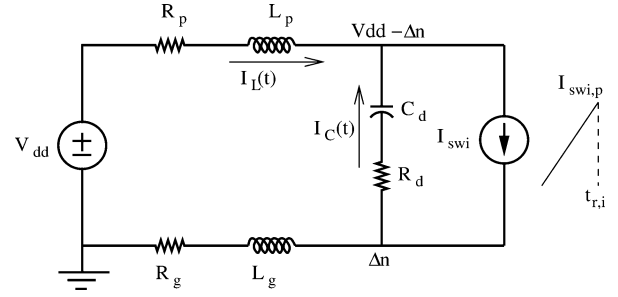


Fig. 5. Equivalent circuit model to estimate power supply noise and ground bounce.  $R_p$ ,  $L_p$ , and  $R_g$ ,  $L_g$  represent the power and ground impedances, respectively.  $C_d$  is the decoupling capacitor and  $R_d$  is the effective series resistance of the capacitor. The load circuit is represented by a current source with a transition time  $t_{r,i}$  and peak current  $I_{swi,p}$ .

digital circuits [2], [23], [24]. Note that this model does not consider the feedback effect of the power noise since in this model the current is independent of this noise. Practically, however, the transistor current is affected by the power noise since this current is dependent upon the power supply [25]. Also note that the impedance between the decoupling capacitor and the current load is negligible, assuming that the decoupling capacitor is placed sufficiently close to the switching circuit [12].

The current provided by the decoupling capacitance  $I_C(t)$  and the current flowing through the parasitic inductance  $I_L(t)$  from the power supply are, respectively

$$I_C(t) = -C_d \frac{\partial V_C}{\partial t} \quad (4)$$

$$I_L(t) = \frac{1}{L_p} \int_0^t V_L(t) \partial t \quad (5)$$

where  $V_C(t)$  and  $V_L(t)$  are, respectively

$$V_C(t) = V_{dd} - 2\Delta n(t) + I_C(t)R_d \quad (6)$$

$$V_L(t) = \Delta n(t) - I_L(t)R_p. \quad (7)$$

Note that the parasitic resistance and inductance of the power and ground networks are assumed to be equal due to the symmetry of these two networks [26], i.e.,  $R_p = R_g$  and  $L_p = L_g$ .

A ramp function is assumed for the noise  $\Delta n(t)$  as

$$\Delta n(t) = \frac{V_{\text{gnd,p}}}{t_{r,v}} t \quad (8)$$

where  $V_{\text{gnd,p}}$  is the peak noise voltage and  $t_{r,v}$  is the transition time of the noise spike [2], [27]. Practically, the noise can be better approximated with an exponential function (due to the discharge from the decoupling capacitor) at the expense of more complicated analytic solutions. The error introduced by approximating the noise as a ramp function is described in Section IV.

Replacing (6) in (4) and (7) in (5), and taking the derivative with respect to time results in the following differential equations:

$$I_C(t) = \frac{2C_d V_{\text{gnd,p}}}{t_{r,v}} - R_d C_d \frac{\partial I_C(t)}{\partial t} \quad (9)$$

$$\frac{\partial I_L(t)}{\partial t} = \frac{V_{\text{gnd,p}}t}{L_g t_{r,v}} - \frac{R_g}{L_g} I_L(t). \quad (10)$$

Solving these differential equations with the initial conditions  $I_C(0) = 0$  and  $I_L(0) = 0$  produces the inductive and capacitive current, respectively, as

$$I_C(t) = V_{\text{gnd,p}} \frac{2C_d}{t_{r,v}} (1 - e^{-t/(R_d C_d)}) \quad (11)$$

$$I_L(t) = V_{\text{gnd,p}} \left[ \frac{t}{t_{r,v} R_g} - \frac{L}{t_{r,v} R_g^2} (1 - e^{-t/L_g/R_g}) \right]. \quad (12)$$

These currents can be rewritten as

$$I_C(t) = G_C(t) V_{\text{gnd,p}} \quad (13)$$

$$I_L(t) = G_L(t) V_{\text{gnd,p}} \quad (14)$$

where  $G_C(t)$ , the conductance of the capacitance path, and  $G_L(t)$ , the conductance of the inductance path, are given, respectively, by

$$G_C(t) = \frac{2C_d}{t_{r,v}} (1 - e^{-t/(R_d C_d)}) \quad (15)$$

$$G_L(t) = \frac{t}{t_{r,v} R_g} - \frac{L_g}{t_{r,v} R_g^2} (1 - e^{-t/L_g/R_g}). \quad (16)$$

Note that these conductances are both a function of the transition time  $t_{r,v}$ . Hence, the amount of current provided by the decoupling capacitor as determined by (13), and the amount of current provided by the power supply as determined by (14) are both dependent upon the transition time. Specifically, as the transition time becomes smaller,  $G_C(t)$  increases and  $G_L(t)$  decreases. This situation is illustrated in Fig. 6 where (15) and (16) are plotted as a function of transition time. The operating parameters are  $I_{\text{swi,p}} = 11.5$  mA,  $L_g = 1$  nH,  $C_d = 10$  pF,  $R_g = 2.2$   $\Omega$ ,  $R_d = 0.1$   $\Omega$ , and  $t = t_{r,v}$ . Note that, in the frequency domain, the admittance of an inductance  $1/j\omega L$  decreases with frequency. A conductance refers to the time-domain correspondence of the admittance. Since a decrease in transition time corresponds to an increase in frequency, the inductive conductance decreases. Similarly, the admittance of a capacitance  $j\omega C$  increases with frequency. In the time domain, therefore, the capacitive conductance increases with decreasing transition time, as illustrated in Fig. 6.

The capacitive current  $I_C(t)$ , therefore, increases with decreasing transition time. Alternatively, the inductive current  $I_L(t)$  increases with longer transition times. Intuitively, a smaller transition time corresponds to a higher frequency, where the impedance of the capacitance is smaller and the inductance is higher. The capacitance is, therefore, more effective at smaller transition times and becomes less effective as the transition time increases since a majority of the switching

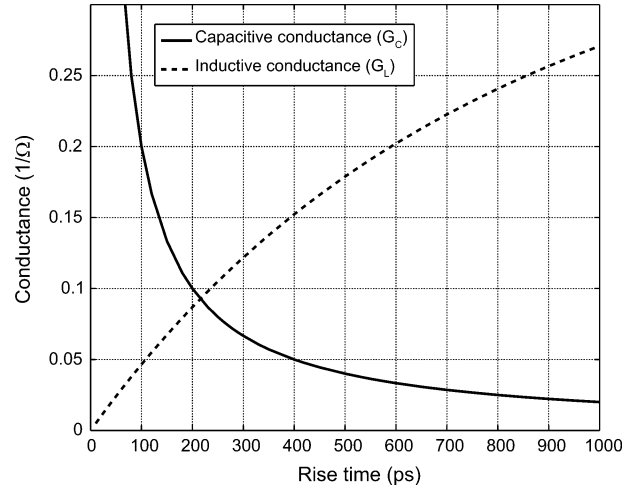


Fig. 6. Capacitive and inductive conductance as a function of rise time where  $I_{\text{swi,p}} = 11.5$  mA,  $L_g = 1$  nH,  $C_d = 10$  pF,  $R_g = 2.2$   $\Omega$ ,  $R_d = 0.1$   $\Omega$ , and  $t = t_{r,v}$ .

current is provided by the power supply at higher transition times. The implications of this dependence are discussed in Section IV.

Assuming the peak ground noise  $V_{\text{gnd,p}}$  occurs when the switching current reaches the maximum current  $I_{\text{swi,p}}$  [2], e.g.,  $t_{r,v} = t_{r,i} = t_r$ , the summation of the capacitive and inductive currents at  $t = t_r$  is equal to the peak switching current  $I_{\text{swi,p}}$  of the load circuit

$$I_{\text{swi,p}} = I_C(t_r) + I_L(t_r). \quad (17)$$

From (13), (14), and (17), the peak ground noise  $V_{\text{gnd,p}}$  at  $t = t_r$  can be expressed as

$$\frac{1}{V_{\text{gnd,p}}} = \frac{G_C(t_r)}{I_{\text{swi,p}}} + \frac{G_L(t_r)}{I_{\text{swi,p}}}. \quad (18)$$

Replacing (15) and (16) in (18) produces the peak noise voltage given in (19), shown at the bottom of the page. Note that if the capacitive current is much greater than the inductive current, e.g., (13)  $\gg$  (14) or (15)  $\gg$  (16), the second term in (18) can be neglected without a significant loss in accuracy, guaranteeing the pessimism of the expression. In this case, the peak ground noise is approximated by

$$V_{\text{gnd,p}} \approx \frac{I_{\text{swi,p}}}{G_C(t_r)}. \quad (20)$$

Alternatively, if the inductive current is much greater, the first term in (18) can be neglected and the peak noise is estimated as

$$V_{\text{gnd,p}} \approx \frac{I_{\text{swi,p}}}{G_L(t_r)}. \quad (21)$$

$$V_{\text{gnd,p}} = \frac{I_{\text{swi,p}} R_g^2 t_r}{2C_d R_g^2 (1 - e^{-t_r/(R_d C_d)}) - L_g (1 - e^{-t_r/L_g/R_g}) + R_g t_r} \quad (19)$$

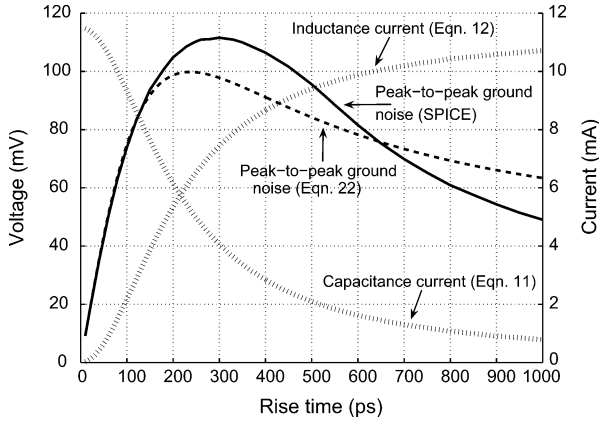


Fig. 7. Comparison of peak-to-peak ground noise as a function of the transition time obtained from SPICE simulations and (22) for  $I_{\text{swi,p}} = 11.5$  mA. The ground network impedances are  $L_g = 1$  nH,  $C_d = 10$  pF,  $R_g = 2.2$   $\Omega$ , and  $R_d = 0.1$   $\Omega$ . The dotted lines depict the estimated capacitive and inductive currents as a function of transition time.

It is, however, important to note that the maximum peak noise occurs when the inductive and capacitive currents are approximately equal, as described in the following section.

If the circuit is underdamped, i.e., the damping factor is smaller than one, oscillations occur due to a parallel combination of the parasitic inductance and decoupling capacitor. In this case, the peak-to-peak ground noise voltage  $V_{\text{gnd,pp}}$  is

$$V_{\text{gnd,pp}} = V_{\text{gnd,p}} \left[ 1 + e^{-\pi\zeta/\sqrt{1-\zeta^2}} \right] \quad (22)$$

where  $\zeta$  is the damping factor given as

$$\zeta = \left[ \frac{(2R_g + R_d)}{2} \right] \sqrt{\frac{C_d}{2L_g}}. \quad (23)$$

#### IV. NONMONOTONIC NOISE BEHAVIOR

The impedance of a parallel  $LC$  circuit is maximum at the resonant frequency,  $\omega = 1/\sqrt{LC}$ . At this frequency, both the capacitive and inductive paths carry a significant amount of current, giving rise to resonant behavior. Similarly, in the time domain, there exists a transition time at which the capacitive and inductive currents are close and the peak-to-peak noise is maximum. The *worst case transition time* producing the maximum noise is described in Section IV-A. The sensitivity of the noise to the decoupling capacitance and parasitic inductance as a function of transition time is explained in Section IV-B.

##### A. Worst Case Transition Time

The capacitive and inductive currents and the corresponding ground noise are plotted as a function of transition time in Fig. 7 using (11) and (12) for the currents and (22) for the noise voltage, where  $I_{\text{swi,p}} = 11.5$  mA,  $L_g = 1$  nH,  $C_d = 10$  pF,  $R_g = 2.2$   $\Omega$ , and  $R_d = 0.1$   $\Omega$ . Equation (22) is also compared with SPICE in Fig. 7.

The model accurately captures the nonmonotonic dependence of noise on transition time, exhibiting a maximum error of 12.5%. Note that this error is due to approximating the noise

as a ramp function which is a better assumption for smaller transition times, producing a smaller error.

As shown in Fig. 7, for sufficiently small transition times, the capacitive current dominates, and the inductance does not affect the ground noise. As the transition time increases, the capacitive current decreases and the inductive current increases. The peak noise occurs at a transition time where these currents are approximately equal. This specific transition time  $t_{r,\text{wc}}$  is referred to as the *worst case transition time* or the *equivalent transition time for resonance* (identical to the resonant behavior in the frequency domain). If the transition time further increases, the noise decreases due to lower  $L \partial i/\partial t$  noise, making the capacitance less significant. The assumption of fast transients as the worst case scenario for noise can be overly optimistic in a circuit with sufficient decoupling capacitance. This conclusion is similar to reducing the resonant frequency with a larger capacitance. Increasing the decoupling capacitance, therefore, has the drawback of reducing the resonant frequency, or similarly, increasing the worst case transition time. Note that the intrinsic capacitance between the power and ground networks due to the nonswitching gates contributes to the overall decoupling capacitance. For sufficiently large circuits, this capacitance can be significant [21], [22], that is, the assumption of fast current transients as the worst case scenario is overly optimistic for large-scale circuits.

According to Fig. 7, an expression for the worst case transition time  $t_{r,\text{wc}}$  can be developed by equating (15) with (16) at  $t = t_r$  and solving for  $t_r$  as

$$G_C(t_{r,\text{wc}}) - G_L(t_{r,\text{wc}}) = 0. \quad (24)$$

A closed-form solution, however, does not exist due to the exponential terms in  $G_C(t_{r,\text{wc}})$  and  $G_L(t_{r,\text{wc}})$ . Assuming  $R_d \rightarrow 0$ , then

$$e^{-t_{r,\text{wc}}/(R_d C_d)} \rightarrow 0. \quad (25)$$

Replacing (25) in (15) gives

$$G_C(t_{r,\text{wc}}) \approx \frac{2C_d}{t_{r,\text{wc}}}. \quad (26)$$

Similarly,  $G_L(t_{r,\text{wc}})$  can be expanded using a Taylor series expansion to

$$G_L(t_{r,\text{wc}}) = \frac{1}{R_g} - \frac{L_g}{t_{r,\text{wc}} R_g^2} \times \left[ 1 - \left( 1 - \frac{t_{r,\text{wc}} R_g}{L_g} \right)^2 + \frac{1}{2!} \left( \frac{t_{r,\text{wc}} R_g}{L_g} \right)^2 + \dots \right] \quad (27)$$

$$G_L(t_{r,\text{wc}}) = \frac{1}{2!} \frac{t_{r,\text{wc}}}{L_g} - \frac{1}{3!} \frac{(t_{r,\text{wc}})^2 R_g}{L_g^2} + \frac{1}{4!} \frac{(t_{r,\text{wc}})^3 R_g^2}{L_g^3} \dots \quad (28)$$

Assuming  $R_g \rightarrow 0$  in (28) results in

$$G_L(t_{r,\text{wc}}) \approx \frac{t_{r,\text{wc}}}{2L_g}. \quad (29)$$

TABLE I  
COMPARISON OF THE PEAK-TO-PEAK GROUND NOISE ANALYTICALLY  
OBTAINED AT  $t_{r,wc} = 2\sqrt{L_g C_d}$  WITH THE PEAK-TO-PEAK NOISE OBTAINED  
BY SPICE FOR DIFFERENT PARASITIC GROUND NETWORK IMPEDANCES

$I_{swi,p}$ mA	$L_g$ (nH)	$C_d$ (pF)	$R_g$ (ohm)	$R_d$ (ohm)	Ground noise at $t_r = 2\sqrt{L_g C_d}$ (mV)	Maximum ground noise (SPICE) (mV)	Error (%)
11.5	0.25	10	2.2	0.1	44	46.2	4.8
11.5	0.5	10	2.2	0.1	66.3	67.8	2.2
11.5	1	10	2.2	0.1	98.5	99.8	1.3
11.5	1	15	2.2	0.1	78.3	79.6	1.6
11.5	1	20	2.2	0.1	66.3	67.8	2.2
11.5	1	20	4	0.1	59.4	64.8	8.3
11.5	1	20	6	0.1	55.1	70.2	21.5
11.5	1	20	6	1	54	68.6	21.3
11.5	1	20	6	2	52.8	67.2	21.4

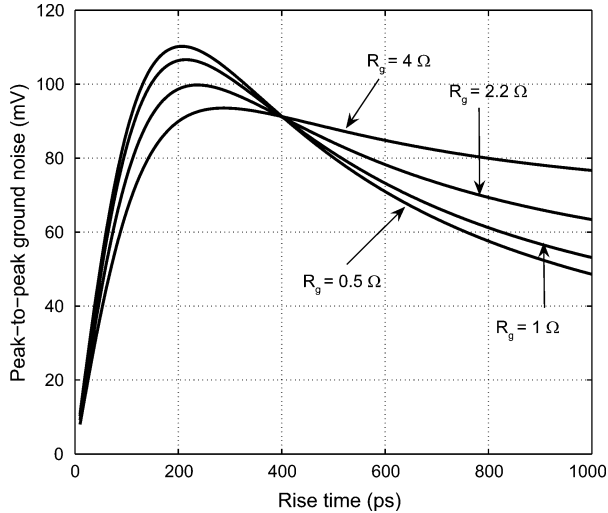


Fig. 8. Peak-to-peak ground noise for different values of  $R_g$  when  $I_{swi,p} = 11.5$  mA,  $L_g = 1$  nH,  $C_d = 10$  pF, and  $R_d = 0.1$  Ω.

The worst case transition time  $t_{r,wc}$  at which these conductances are approximately equal is determined from (26) and (29) as

$$\frac{2C_d}{t_{r,wc}} = \frac{t_{r,wc}}{2L_g} \implies t_{r,wc} = 2\sqrt{L_g C_d}. \quad (30)$$

The ground noise is obtained at  $t_{r,wc} = 2\sqrt{L_g C_d}$  for different parasitic impedances of the ground network and compared with the maximum noise obtained at the same impedance. These results are listed in Table I. The error of  $t_{r,wc} = 2\sqrt{L_g C_d}$  in estimating the maximum noise is greater with increasing  $R_g$  and  $R_d$ , but is sufficiently small within the practical values of these resistances, as listed in Table I.

The effect of the parasitic resistance  $R_g$  and the effective series resistance of the decoupling capacitance  $R_d$  on the worst case transition time is further illustrated, respectively, in Figs. 8 and 9. Increasing  $R_g$  reduces the noise until a specific transition time is reached due to additional damping. Beyond this transition time, however, the noise increases due to a greater  $IR$  drop along the ground network, making the decoupling capacitance ineffective. Alternatively, an increase in  $R_d$  results in decreased noise at higher transition times due to the increased damping and higher noise at smaller transition times where the decoupling capacitance is effective.

### B. Noise Sensitivity as a Function of Transition Time

The normalized sensitivity of the ground noise as a function of transition time is determined in this section to evaluate the

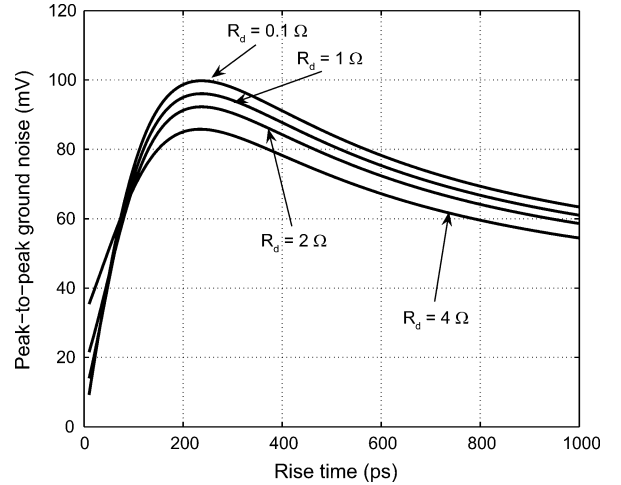


Fig. 9. Peak-to-peak ground noise for different values of  $R_d$  when  $I_{swi,p} = 11.5$  mA,  $L_g = 1$  nH,  $C_d = 10$  pF, and  $R_g = 2.2$  Ω.

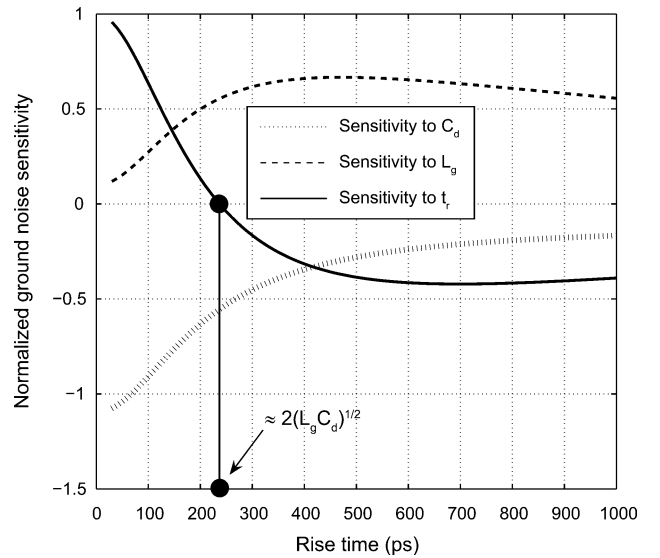


Fig. 10. Normalized sensitivity of the ground noise as a function of transition time when  $I_{swi,p} = 11.5$  mA,  $L_g = 1$  nH,  $C_d = 10$  pF,  $R_g = 2.2$  Ω, and  $R_d = 0.1$  Ω.

efficacy of reducing the parasitic inductance and increasing the decoupling capacitance on reducing the ground noise. The normalized sensitivity of the ground noise to a parameter  $p_i$  is determined by

$$S_{p_i}^{V_{gnd,pp}} = \lim_{\Delta p_i \rightarrow 0} \frac{\frac{\Delta V_{gnd,pp}}{V_{gnd,pp}}}{\frac{\Delta p_i}{p_i}} = \frac{p_i}{V_{gnd,pp}} \frac{\partial V_{gnd,pp}}{\partial p_i}. \quad (31)$$

The normalized sensitivity of the ground noise as a function of transition time, as determined by (31), is shown in Fig. 10. The sensitivity of the noise to the decoupling capacitance is high at small transition times and decreases with increasing transition time. Alternatively, the sensitivity of the noise to the parasitic inductance is low at small transition times and increases with longer transition times. Increasing the decoupling capacitance is therefore effective in reducing the noise for  $t_r \leq 2\sqrt{L_g C_d}$ . Alternatively, reducing the parasitic inductance is effective for

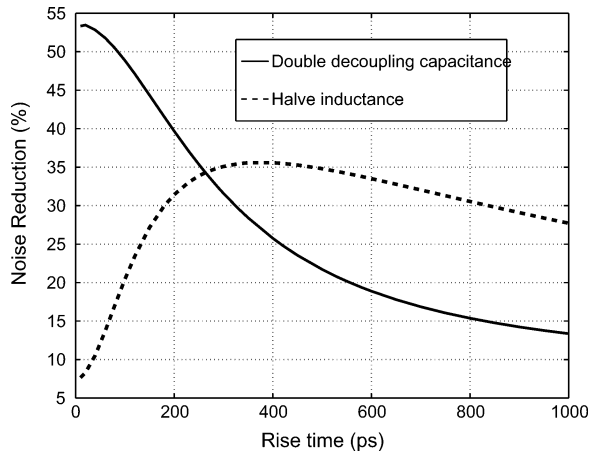


Fig. 11. Comparison of the noise reduction obtained by doubling the decoupling capacitance and halving the inductance.

TABLE II

EFFECT OF THE DECOUPLING CAPACITANCE ON REDUCING THE PEAK-TO-PEAK GROUND NOISE.  $L_g = 1$  nH

Transition time (ps)	$C_d = 10$ pF	$C_d = 20$ pF	Reduction
70	57.8	28.2	51.2%
$200 = 2\sqrt{L_g C_d}$	98.7	59.5	39.7%
400	91.1	67.7	25.7%
800	69.4	58.7	15.4%

TABLE III

EFFECT OF THE PARASITIC INDUCTANCE ON REDUCING THE PEAK-TO-PEAK GROUND NOISE.  $C_d = 10$  pF

Transition time (ps)	$L_g = 1$ nH	$L_g = 0.5$ nH	Reduction
70	57.8	48.9	15.4%
$200 = 2\sqrt{L_g C_d}$	98.7	67.7	31.4%
400	91.1	58.7	35.6%
800	69.4	48.2	30.5%

$t_r \geq 2\sqrt{L_g C_d}$ . This behavior is due to the changing ratio of the capacitive and inductive currents with respect to the transition time, as shown in Fig. 7. The effect of the decoupling capacitance and parasitic inductance on the ground noise is listed, respectively, in Tables II and III for different transition times. At  $t_r = 70$  ps, doubling the decoupling capacitance reduces the noise by 51.2%, and only 25.7% when  $t_r = 400$  ps. Halving the parasitic inductance, however, reduces the noise by only 15.4% when  $t_r = 70$  ps, and 35.6% when  $t_r = 400$  ps. Note that the sensitivity to the transition time crosses over at zero when  $t_r \approx 2\sqrt{L_g C_d}$ , demonstrating the nonmonotonic dependence, as described in Section IV-A. Placing additional decoupling capacitance is therefore more effective in reducing the noise at smaller rise times. Alternatively, reducing the parasitic inductance is more effective at higher transition times. This behavior is illustrated in Fig. 11.

## V. CONCLUSION

The nonmonotonic dependence of the power/ground noise on the transition time is shown for an inductive power distribution network with a decoupling capacitance. The power/ground interconnect is modeled as a series  $RL$  impedance. The decoupling capacitance is modeled as a capacitance in series with a resistance. The model captures the nonmonotonic dependence of

noise on the transition time with sufficient accuracy as compared to SPICE. The *worst case transition time* or the *equivalent transition time for resonance* producing the maximum peak-to-peak noise is also presented based on this model. The worst case power/ground noise is shown to be significantly inaccurate if determined assuming fast switching characteristics. The effect of the parasitic line resistance  $R_g$  and effective series resistance  $R_d$  of the decoupling capacitor on the noise is also investigated. Increasing  $R_g$  reduces the noise at smaller transition times due to additional damping since the decoupling capacitance is effective. At higher transition times, however, the noise increases due to a larger  $IR$  drop along the inductive power/ground path. Alternatively, an increase in  $R_d$  results in lower noise at higher transition times by providing additional damping and higher noise at lower transition times due to a larger  $IR$  drop along the capacitive path. The sensitivity of the noise on the decoupling capacitance and parasitic inductance is also investigated. The decoupling capacitance is shown to efficiently reduce the noise for transition times smaller than twice the  $LC$  time constant,  $t_r \leq 2\sqrt{L_g C_d}$ . Alternatively, reducing the parasitic inductance is effective for transition times greater than twice the  $LC$  time constant,  $t_r \geq 2\sqrt{L_g C_d}$ .

## REFERENCES

- [1] M. Popovich, A. V. Mezhiba, and E. G. Friedman, *Power Distribution Networks With On-Chip Decoupling Capacitors*. Berlin, Germany: Springer-Verlag, 2008.
- [2] P. Larsson, "di/dt noise in CMOS integrated circuits," *Analog Integr. Circuits Signal Process.*, vol. 14, no. 2, pp. 113–129, Sep. 1997.
- [3] S. N. Lalgudi, M. Swaminathan, and Y. Kretschmer, "On-chip power-grid simulation using latency insertion method," *IEEE Trans. Circuits Syst. I, Reg. Papers*, vol. 55, no. 4, pp. 914–931, Apr. 2008.
- [4] M. Saint-Laurent and M. Swaminathan, "Impact of power-supply noise on timing in high-frequency microprocessors," *IEEE Trans. Adv. Packag.*, vol. 27, no. 1, pp. 135–144, Feb. 2004.
- [5] E. Alon, V. Stojanovic, and M. A. Horowitz, "Circuits and techniques for high resolution measurement of on-chip power supply noise," *IEEE J. Solid-State Circuits*, vol. 40, no. 11, pp. 820–828, Nov. 2005.
- [6] L. H. Chen, M. Marek-Sadowska, and F. Brewer, "Buffer delay change in the presence of power and ground noise," *IEEE Trans. Very Large Scale Integr. (VLSI) Syst.*, vol. 11, no. 3, pp. 461–473, Jun. 2003.
- [7] M. Favalli and L. Benini, "Analysis of glitch power dissipation in CMOS ICs," in *Proc. IEEE Int. Symp. Low Power Design*, Apr. 1995, pp. 123–128.
- [8] A. Strak, A. Gothenberg, and H. Tenhunen, "Power-supply and substrate-noise-induced timing jitter in nonoverlapping clock generation circuits," *IEEE Trans. Circuits Syst. I, Reg. Papers*, vol. 55, no. 4, pp. 1041–1054, May 2008.
- [9] S. H. Hashemi, P. A. Sandborn, D. Disko, and R. Evans, "The close attached capacitor: A solution to switching noise problems," *IEEE Trans. Compon., Hybrids, Manuf. Technol.*, vol. 15, no. 6, pp. 1056–1063, Dec. 1992.
- [10] L. D. Smith, R. E. Anderson, D. W. Forehand, T. J. Pelc, and T. Roy, "Power distribution system design methodology and capacitor selection for modern CMOS technology," *IEEE Trans. Adv. Packag.*, vol. 22, no. 4, pp. 284–291, Aug. 1999.
- [11] C. Y. Yeh and M. M. Sadowska, "Timing-aware power-noise reduction in placement," *IEEE Trans. Comput.-Aided Design Integr. Circuits Syst.*, vol. 26, no. 3, pp. 526–541, Mar. 2007.
- [12] M. Popovich, M. Sotman, A. Kolodny, and E. G. Friedman, "Effective radii of on-chip decoupling capacitors," *IEEE Trans. Very Large Scale Integr. (VLSI) Syst.*, vol. 16, no. 7, pp. 894–907, Jul. 2008.
- [13] H. Yamamoto and J. A. Davis, "Decreased effectiveness of on-chip decoupling capacitance in high-frequency operation," *IEEE Trans. Very Large Scale Integr. (VLSI) Syst.*, vol. 15, no. 6, pp. 649–659, Jun. 2007.
- [14] P. Larsson, "Resonance and damping in CMOS circuits with on-chip decoupling capacitance," *IEEE Trans. Circuits Syst. I, Fundam. Theory Appl.*, vol. 45, no. 8, pp. 849–858, Aug. 1998.

- [15] H. H. Chen and J. S. Neely, "Interconnect and circuit modeling techniques for full-chip power supply noise analysis," *IEEE Trans. Compon., Packaging, Manuf. Technol.*, vol. 21, no. 3, pp. 209–215, Aug. 1998.
- [16] M. Badaroglu *et al.*, "Evolution of substrate noise generation mechanisms with CMOS technology scaling," *IEEE Trans. Circuits Syst. I, Reg. Papers*, vol. 53, no. 2, pp. 296–305, Feb. 2006.
- [17] G. Konstantinidis *et al.*, "Implementation of a third-generation 16-Core 32-thread chip-multithreading SPARC processor," in *Proc. IEEE Int. Solid-State Circuits Conf.*, Feb. 2008, pp. 84–85.
- [18] L. D. Smith, "Decoupling capacitor calculations for CMOS circuits," in *Proc. IEEE Conf. Elect. Performance of Electron. Packaging*, Nov. 1994, pp. 101–105.
- [19] C. R. Paul, "Effectiveness of multiple decoupling capacitors," *IEEE Trans. Electromagn. Compatibil.*, vol. 34, no. 2, pp. 130–133, May 1992.
- [20] J. Chen and L. He, "Efficient in-package decoupling capacitor optimization for I/O power integrity," *IEEE Trans. Comput.-Aided Design Integr. Circuits Syst.*, vol. 26, no. 4, pp. 734–738, Apr. 2007.
- [21] M. Sotman, M. Popovich, A. Kolodny, and E. G. Friedman, "Leveraging symbiotic on-die decoupling capacitance," in *Proc. IEEE Top. Meet. Elect. Performance of Electronic Packaging*, Oct. 2005, pp. 111–114.
- [22] M. Badaroglu *et al.*, "Digital circuit capacitance and switching analysis for ground bounce in ICs with a high-ohmic substrate," *IEEE J. Solid-State Circuits*, vol. 39, no. 7, pp. 1119–1129, Jul. 2004.
- [23] M. Badaroglu *et al.*, "Clock skew optimization methodology for substrate noise reduction with supply current folding," *IEEE Trans. Comput.-Aided Des. Integr. Circuits Syst.*, vol. 25, no. 6, pp. 1146–1154, Jun. 2006.
- [24] N. Srivastava, X. Qi, and K. Banerjee, "Impact of on-chip inductance on power distribution network design for nanometer scale integrated circuits," in *Proc. IEEE Int. Symp. Quality Electron. Design*, Mar. 2005, pp. 346–351.
- [25] R. Senthinathan, G. Tubbs, and M. Schuelein, "Negative feedback influence in simultaneously switching CMOS outputs," in *Proc. IEEE Custom Integr. Circuits Conf.*, May 1988, pp. 5.4.1–5.4.5.
- [26] R. Panda *et al.*, "Model and analysis for combined package and on-chip power grid simulation," in *Proc. IEEE Int. Symp. Low Power Electron. Design*, Jul. 2000, pp. 179–184.
- [27] Y. Yang and J. R. Brews, "Design trade-offs for the last stage of an unregulated long-channel CMOS off-chip driver with simultaneous switching noise and switching time considerations," *IEEE Trans. Compon., Packaging, Manuf. Technol.*, vol. 19, no. 3, pp. 481–486, Aug. 1997.



**Emre Salman (S'04)** received the B.S. degree in microelectronics engineering from Sabanci University, Istanbul, Turkey, in 2004 and the M.S. degree in electrical and computer engineering and the Ph.D. degree in electrical engineering from the University of Rochester, Rochester, NY, in 2006 and 2009, respectively.

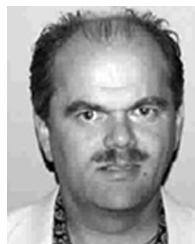
He was a cooperative student with STMicroelectronics, Istanbul, Turkey, between October 2003 and May 2004, where he worked on the design and verification of a clock and data recovery circuit for a multi-channel fiber-optic transceiver. In the summer of 2005, he interned at Synopsys Inc., Mountain View, CA, where he worked on pessimism reduction in static timing analysis (STA) and cell library characterization. During the summers of 2006 and 2007, he was with Freescale Semiconductor Corporation, Tempe, AZ, where he worked on circuit- and physical-level signal isolation methodologies with application to monolithic transceivers in CMOS and BiCMOS technologies. His research interests include analysis, modeling, and design methodologies for high-performance digital and mixed-signal integrated circuits, focusing on switching noise and timing characteristics, signal and power integrity, and the design of on-chip global interconnects such as power and clock networks.



**Eby G. Friedman (F'00)** received the B.S. degree from Lafayette College, Lafayette, PA, in 1979, and the M.S. and Ph.D. degrees from the University of California, Irvine, in 1981 and 1989, respectively, all in electrical engineering.

From 1979 to 1991, he was with Hughes Aircraft Company, rising to the position of Manager of the Signal Processing Design and Test Department, responsible for the design and test of high performance digital and analog IC's. He has been with the Department of Electrical and Computer Engineering, University of Rochester, Rochester, NY, since 1991, where he is a Distinguished Professor and the Director of the High Performance VLSI/IC Design and Analysis Laboratory. He is also a Visiting Professor with the Technion—Israel Institute of Technology, Haifa. His current research and teaching interests are in high-performance synchronous digital and mixed-signal microelectronic design and analysis with application to high-speed portable processors and low power wireless communications. He is the author of more than 325 papers and book chapters, several patents, and the author or editor of ten books in the fields of high-speed and low-power CMOS design techniques, high-speed interconnect, and the theory and application of synchronous clock and power distribution networks.

Dr. Friedman is a Senior Fulbright Fellow. He is the Regional Editor of the *Journal of Circuits, Systems and Computers*, a Member of the editorial boards of the *Analog Integrated Circuits and Signal Processing*, *Microelectronics Journal*, *Journal of Low Power Electronics*, and *Journal of Signal Processing Systems*, Chair of the IEEE TRANSACTIONS ON VERY LARGE SCALE INTEGRATION (VLSI) SYSTEMS steering committee, and a Member of the technical program committee of a number of conferences. He previously was the Editor-in-Chief of the IEEE TRANSACTIONS ON VERY LARGE SCALE INTEGRATION (VLSI) SYSTEMS, a Member of the editorial board of the PROCEEDINGS OF THE IEEE and the IEEE TRANSACTIONS ON CIRCUITS AND SYSTEMS II: ANALOG AND DIGITAL SIGNAL PROCESSING, a Member of the IEEE Circuits and Systems (CAS) Society Board of Governors, Program and Technical chair of several IEEE conferences, Guest Editor of several special issues in a variety of journals, and a recipient of the University of Rochester Graduate Teaching Award, and a College of Engineering Teaching Excellence Award.



**Radu M. Secareanu (M'00)** received the Ph.D. degree from the University of Rochester, Rochester, NY, in 2000.

Prior to beginning his doctoral work, he was a Design R&D Engineer for five years. Since 2000, he has been with the Microwave and Mixed-Signal Technologies Laboratory, Freescale Semiconductor (formerly Motorola SPS), Tempe, AZ. Since 2002, he has also been an Adjunct Professor with the Electrical Engineering Department, Arizona State University, Tempe. His research interests include signal integrity (substrate, interconnect, and power-ground network) and the relationship with new technologies and mixed-signal and RF circuit design aspects, and low-voltage and low-power circuit design. He has authored and coauthored over 30 referred papers and five issued and six pending patents. He has served in several conference committees, has presented several conference tutorials, and is actively involved in Semiconductor Research Corporation (SRC) activities.

Mr. Radu was a recipient of one of the 2007 Mahboob Khan Outstanding Mentor Awards. He has served as an Associate Editor for the IEEE TRANSACTIONS ON VERY LARGE SCALE INTEGRATION (VLSI) SYSTEMS.



**Olin L. Hartin** was born in Seminole, TX. He received the Ph.D. degree from the University of Texas at Austin.

He has lead the Device Physics and Simulation Group with Motorola and then Freescale Semiconductor, Tempe, AZ, for the last eight years. His technical contributions have been mainly in small- and large-signal RF device and circuit design.